Dalton Transactions

Accepted Manuscript

ROYAL SOCIETY OF CHEMISTRY

www.rsc.org/dalton

Journal Name

ARTICLE

Novel $La_3Fe(MoO_4)_6$ phase: magnetic properties and ethanol reactivity

Received 00th January 20xx,
Accepted 00th January 20xx

DOI: 10.1039/x0xx00000x

www.rsc.org/

Marie Colmont[a*], Georgiana Bucataru[a], Anita Borowiec[a], Mickaël Capron[a], Franck Dumeignil[a,b], Marielle Huvé[a], Frédéric Capet[a], Françoise Damay[c], Olivier Mentré[a] and Pascal Roussel[a]

Single crystals of the new oxide $La_3Fe(MoO_4)_6$ were grown from fluxes of oxide precursors, and a polycrystalline sample was also prepared by a standard solid state reaction. $La_3Fe(MoO_4)_6$ crystallizes in the orthorhombic space group Pbca with unit cell parameters a = 19.3164(11), b = 10.4143(5) and c = 22.0594(12) Å. This crystal structure exhibits a singular architectural type built on infinite chains of $Fe(MoO_4)_4$, each of them being surrounded by two isolated MoO_4 tetrahedra and three isolated La^{3+} cations. Fe^{3+} ions in $La_3Fe(MoO_4)_6$ are antiferromagnetically ordered below TN = 6.6 K in chains and between chains, as refined from neutron diffraction data. Further the redox stability of this compound - pure powder – was checked using temperature-programmed X-ray diffraction under controlled atmosphere: under air, we observed a reversible phase transition above 523K. The same phenomenon was observed under reductive atmosphere, followed by a destruction of the as-formed phase above 923K owing to iron III to II reduction. Reactivity of ethanol was then evaluated to get insights on the redox properties of the material under working conditions. After 4 hours of reaction at 648K, the ethanol conversion was 97 % with a selectivity to acetaldehyde of ~ 60 %, the other products being formaldehyde (~ 10 %) and CO_2 (~ 30 %), underlining a better acetaldehyde selectivity than that of the La-free conventional $Fe_2(MoO_4)_3$ catalytic formulation.

Introduction

The prospection for new inorganic materials is usually driven by the ulterior motive of increasing performances of particular applications. The scientists dream about the possibility to design new materials with targeted properties. Nevertheless, if developing a predictive strategy route is a smart approach, it is pretty often unsuccessful due to technical difficulties for synthesis and because the properties are often not as promising as thought. In this context, the nature of the atoms inherent to the material itself was tuned and their association in the structure studied enabling properties modification. For example, piezo-electricity, pyroelectricity, and ferroelectricity **[1]**,**[2]** properties are strongly related to the achievement of noncentrosymmetric (NCS) **[3]** compounds favored by introduction of lone-pair (LP) cations or polyanions inducing an external s2 electron favorably arranged in NCS crystal structures **[4]**,**[5]**. Rational substitution of a cation by another one less charged that will thus induce vacancies in the structure is the classical technique used to increase ionic conductivity in materials **[6]**. This modification can further potentially lead to changes in the catalytic reactivity of the as-formed compounds.

Catalytic conversion of alcohols is nowadays of topical interest, as some of them are readily obtained from bio resources. Among them, ethanol is now massively produced for biofuels needs, but it is also being more and more considered as a platform molecule from which families of chemicals can be derived. **[7]** For instance, ethanol can be used as a starting material in the synthesis of different byproducts such as aldehydes **[8]**,**[9]**, acetals **[10]**,**[11]**, ethers, esters or alcohols with longer carbonated chains through the Guerbet chemistry **[12]**,**[13]**. Such products are then of high importance in the context of the biorefineries development, as intermediate reactants in the downstream production of alternative fuel or chemicals. **[14]** Within this frame, FeMo-based mixed oxides (namely $Fe_2(MoO_4)_3$) are known for their specific redox behavior making them good catalysts for alcohols oxidation **[15]**,**[16]**.

In the present paper, we synthesized and characterized the structure of a new lanthanum molybdenum iron oxide $La_3Fe(MoO_4)_6$. As preliminary study, AFM coupling at very low temperature were evidenced. Further, we examined the catalytic properties of this new material including La in a FeMo oxide-based host structure. On a mechanically milled compound, a conversion of 97 % was observed at 650K with a selectivity to acetaldehyde of 62 %.This clearly outperforms a conventional FeMo catalyst, which exhibits a much lower selectivity to acetaldehyde due to uncontrolled ethanol reaction from *ca*. 575K.

[a] *Université Lille 1 Sciences et Technologies, UMR 8181 CNRS, Unité de Catalyse et Chimie du Solide 'UCCS', F-59655 Villeneuve d'Ascq, France.*
[b] *Institut Universitaire de France, Maison des Universités, 103 Bd St-Michel, Paris, 75005, France.*
[c] *Laboratoire Léon Brillouin, UMR12, CEA Saclay, CEA-CNRS, 91191 Gif sur Yvette Cedex, France.*
† Email: marie.colmont@ensc-lille.fr.
Electronic Supplementary Information (ESI) available: [details of any supplementary information available should be included here]. See DOI: 10.1039/x0xx00000x

Experimental section

Synthesis of $La_3Fe(MoO_4)_6$: Single crystals: The flux growth technique was used to obtain single crystals. Indeed, this method has been shown to be particularly well suited in the exploratory crystal growth and discovery of novel complex oxides **[17]**. The temperature of synthesis is imposed by the nature of the inorganic chemical used as the solvent for crystallization, here MoO_3.

The crystals were found in the polycrystalline residue from the melt of 34 wt% of the (80% $La(OH)_3$ + 10% Cr_2O_3 + 10% Fe_2O_3) mixture in 66 (wt%) of MoO3 which was taken as a flux. The protocol of heat treatment was deduced from the careful examination of ref. **[17]**. The starting mixture was loaded into a gold tube, sealed and then heated at 1175K during 96 hours and finally slowly cooled (40ºC/h) during 20h. The furnace was then switched off and crystals were handily selected under a 60x Nikon binocular.

Powder sample: The corresponding powder was obtained as a pure polycrystalline phase from the stoichiometric mixture of $La(OH)_3$ (preferred to La_2O_3 which is highly hygroscopic) and Fe_2O_3 and MoO_3 heated at 1175K in an alumina crucible, after several

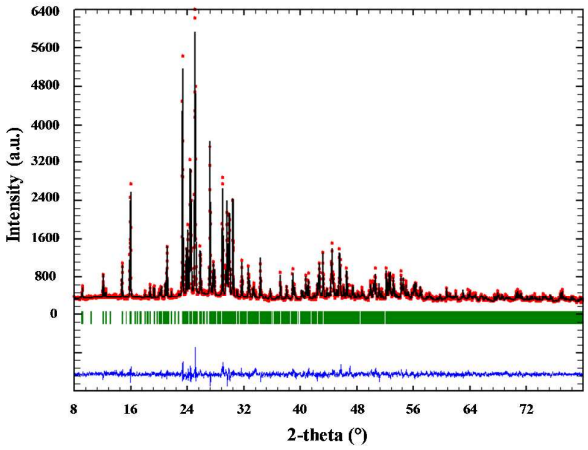

Figure 1: XRD profile and Rietveld refinement for $La_3Fe(MoO_4)_6$ with refined parameters a= 19.3212(3) Å b= 10.4381(2) and c= 22.1252(3) Å at RT.

intermediate grindings. The sample was promptly removed from the furnace at elevated temperature to avoid any residual presence of Fe_2O_3. $La_3Fe(MoO_4)_6$ was obtained as a single phase, as proved by the good pattern matching shown in Figure 1. The lattice parameters refined from this powder diffraction pattern (using JANA 2006 software **[18]**) led to a=19.3212(3) Å b=10.4381(2) Å and c=22.1252(3) Å in good agreement with the lattice parameters refined from the single crystal data (see below).

Structural characterization:

Single crystal XRD study: Single crystals of this new phase have been collected using a Bruker Apex Duo diffractometer with a Mo-IμS microfocus tube (λ=0.71073 Å). The intensity data have been extracted from the collected frames using the program SAINT-Plus 8.27b.**[19]** The lattice parameters have been refined from the complete data set. Absorption corrections have been performed using multiscan methods using SADABS.**[20]** The crystal structure was solved by charge flipping method using SUPERFLIP **[21]** and the data was refined with the JANA2006 **[18]** crystallographic suite. After absorption correction, the 10170 reflections (I>3σ(I)) were merged in the Laue group mmm leading to merging factor Rint=3.2% for 8270 reflections with I>3σ(I). The refined orthorhombic lattice parameters of the titled compound are: a=19.3164(11) Å, b=10.4143(5) Å, c=22.0594(12) Å. Analysis of the data set revealed that the systematic absences were consistent with the orthorhombic space group Pbca. All relevant details of data collection and pertinent data of the refinements are gathered in Table S1.

X-ray powder diffraction analysis of the powder sample has been performed at room temperature in the angular range of 2θ 1-80° with the scan step width of 0.02° using a D8 Advance Bruker AXS diffractometer in Bragg Brentano geometry equipped with a 1D LynxEye detector. Full pattern matching was performed on JANA 2006.**[18]**

High-temperature X-ray diffraction (HTXRD): The temperature stability of the title compound was checked using HTXRD techniques on a Bruker D8 Advance diffractometer equipped with a high-temperature Anton Paar XRK900 chamber and a one dimensional X-ray detector (LynxEye) using Cu Kα radiation under two different atmospheres, namely air and diluted H_2/N_2 (3%) to simulate an oxidative and a reductive media, respectively. Data were collected over the range 10-70° in 2θ, with a 0.021° step and a time of 59min per diagram from room temperature to 1075K. Diffractograms were obtained every 50K on heating and cooling.

Textural characterization: The specific surface areas (SSAs) of the calcined catalysts were determined using the single-point BET (Brunauer, Emmett, Teller) method, with N_2 adsorption at liquid N_2 temperature and subsequent desorption at room temperature on a Micromeritics ASAP 2010 apparatus. The samples were outgassed at 473 K for 30 minutes prior to analysis.

Magnetic characterization: Magnetic susceptibility was measured using a MPMS SQUID-VSM (Quantum Design) magnetometer. The temperature dependence variation of the magnetization was carried out under a magnetic field of 0.1 T after cooling the sample in a field of 0.1 T (FC, field cooling) or in zero field (ZFC, zero field cooling). Magnetization versus H was measured between +3 and -3 T at 2 K.

Magnetic structure: Neutron diffraction experiments (ND) were carried out from room temperature to low temperature (1.5K) on the G4.1 beam line of LLB (Saclay, France) with a wavelength λ=2.43 Å. The ND patterns were recorded in the angular range 2θ=9–80° with a 0.05° step, using approximately 8 g of powder introduced in a vanadium tubular sample holder.

Catalytic test: Materials and apparatus: Reaction of ethanol oxidation was performed using a fixed bed reactor. Before the experiment, 200 mg of sample was mixed with 200 mg of SiC in order to homogenize the temperature inside the catalytic bed. The catalytic tests were carried out in a glass reactor consisting of a 10 mm diameter tube connected online with a GC-MS apparatus, which enabled analysis runs every 3 min. The reactor was placed in

an oven of which the temperature was finely controlled using two thermocouples. The reaction was performed in a range of temperatures between 600 and 675°C under atmospheric pressure. The total gas flow rate was maintained with a GHSV of 2256 h^{-1}

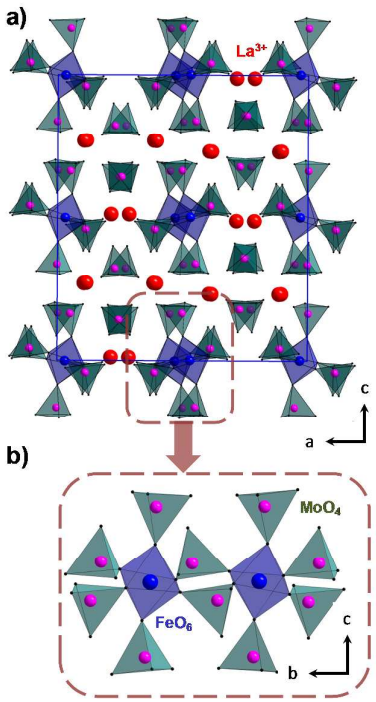

Figure 2: a) Projection of the structure of $La_3Fe(MoO_4)_6$, along the b axis. It is built on isolated MoO_4 tetrahedra (dark green), isolated La^{3+} cations and $Fe(MoO_4)_6$ infinite chains b) shown along a axis.

during the reaction, and the gas composition was kept as 13.2 Vol.% of ethanol, 6 Vol.% of oxygen and 40.8 Vol.% of helium taken as a carrier gas. The catalytic performances were evaluated by calculating the following parameters:

Ethanol conversion (%): $\boldsymbol{X = \frac{(n^0 - n)\cdot 100}{n^0}}$,

where n^0 is the initial number of moles of ethanol and n is the number of moles of unconverted ethanol.

Selectivity to products (%): $\boldsymbol{S = \frac{n_{Cx}\cdot n_x}{n_{CEth}(n^0 - n)}}$,

where n_{Cx} is the number of carbons in the x product, nx the number of moles of the formed x product, and n_{CEth} the number of carbon atoms in one ethanol molecule (i.e., 2).

Crystal structure of $La_3Fe(MoO_4)_6$

A colourless needle like single crystal was isolated from the inhomogeneous melt and mounted on a glass fibre. As aforementioned, the observed extinction conditions undoubtedly suggest the Pbca space group. The heavy atoms (3 La, 6 Mo and 1 Fe atoms) were easily localized using the Superflip21 method, whereas the remaining atoms (24 O) were deduced from the inspection of successive difference Fourier maps. The structure refinement rapidly converged to the conventional reliability factor R_1= 0.0218.

The refined obtained crystal structure is shown on figure 2. It can be described as an association of one dimensional (1D) chains of $[Fe(MoO_4)_6]$, running along the b-axis, the chains being themselves built through the connection of FeO_6 octahedra (dFe-O from 1.9124(20) to 2.0132(18) Å) sharing corners with four MoO_4 (dMo-O from 1.719 (2) to 1.8032(19)Å) tetrahedra. These chains are surrounded by cationic tunnels hosting La^{3+} (2 independent crystallographic sites so 16 cations per unit cell along b-axis) and isolated MoO_4 tetrahedra. The resulting electroneutral formula is $La_3Fe(MoO_4)_6$. In this (La Fe Mo O) quaternary system, this compound is, beside $La(Fe_{0.667}Mo_{0.333})O_3$.**[22]**, the second one referenced in the ICSD database.

The 1D $[Fe(MoO_4)_6]$ units encountered in the title compound can be compared to other iron molybdenum oxides reported in literature. $Rb_3FeMo_4O_{15}$ **[23]** exhibit 1D $Fe[Mo_4O_{15}]$ chains more or less identical but with one oxygen atom in common with two MoO_4 tetrahedra (figure 3a)). FeO_6 octahedra and MoO_4 tetrahedra are also involved in 2D layers in $KFe(MoO_4)_2$ **[24]** by sharing corners (figure 3b)). In the other three examples: $Fe_2(MoO_4)_3$ (figure 3d)) **[25]**, $Cs_2Fe_2(MoO_4)_3$ (figure 3c))**[26]** and $Cs_3FeMo_4O_{15}$ (figure 3e)) **[23]**, the connectivity between iron octahedra and molybdenum tetrahedra is realized by assembling oxygen corners together, building a final 3D framework, more or less distorted by co-addition of counter cations.

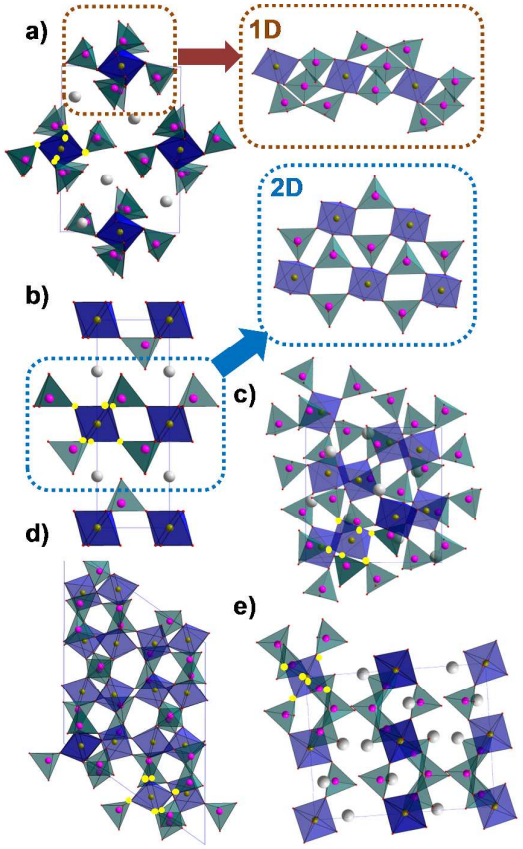

Figure 3: Several connections between FeO_6 octahedra and MoO_4 tetrahedra observed in the literature and compared to $La_3Fe(MoO_4)_6$. a) $Rb_3FeMo_4O_{15}$ building 1D units (corner sharing between FeO_6 and MoO_4 tetrahedra are highlighted in yellow), b) $FeK(MoO_4)_2$ with 2D $Fe(MoO_4)_2$ cationic layers and finally c) $Cs_2Fe_2(MoO_4)_3$, d) $Fe_2(MoO_4)_3$ and e) $Cs_3Fe(Mo_4O_{15})$ building a 3D network.

and another set of MoO_4 tetrahedra. Such arrangement is also closely related to the rather large unit-cell volume ($V=4437.62(41)Å^3$).

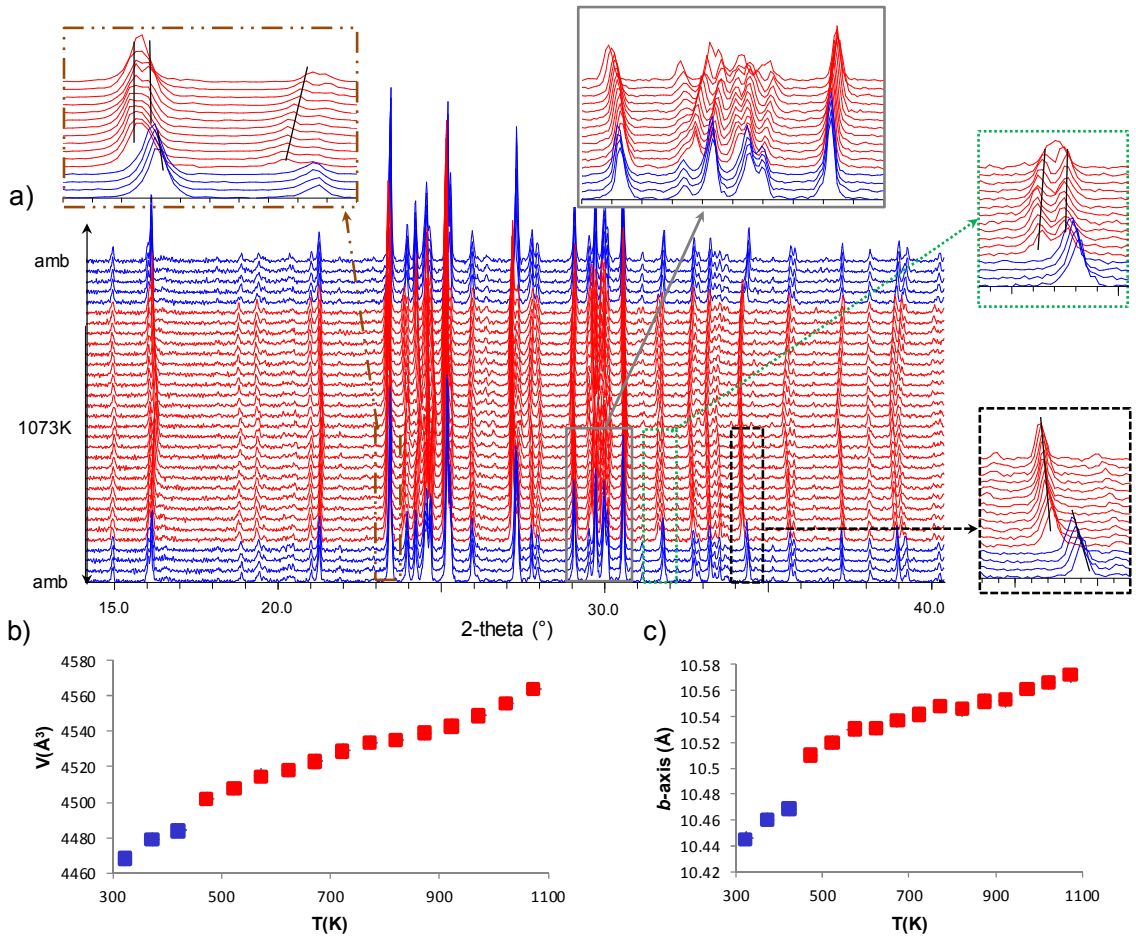

Figure 4: a) High-temperature X-ray diffraction data for $La_3Fe(MoO_4)_6$. A reversible transition is observed at 523K during the heating and cooling process as shown on inserts, blue diagrams correspond to the initial phase and red ones to the HT phase, b) cell volume and c) *b*-axis parameter evolution versus temperature for $La_3Fe(MoO_4)_6$ giving the thermal expansion coefficient.

The atomic positions, anisotropic displacement parameters and the principal distances are given in Supplementary Information S2 and S3. The crystal-structure data for $La_3Fe(MoO_4)_6$ phase were deposited with the depository number CSD-429247.

Structural complexity of $La_3Fe(MoO_4)_6$ structure has been quantified using Shannon information theory **[27]**. Theoretically, structural complexity is strongly related to the atomic arrangement of the unit cell and using Shannon' law. I_G,total is equal to 1383.79 bits per unit cell (bit/u.c.), which classifies it as a very complex structure. It is noteworthy that, only 0.02% of inorganic structures are identified as very complex as detailed in **[27]**. Here the complexity is due to the chemical composition and the number of isolated groups gathered in the structure in terms of rods of FeO_6 octahedra + 6 MoO_4 sharing corners and isolated by La^{3+} cations

High temperature X-Ray study and stability

To simulate the different cycles and to check the stability of the solid prior to catalytic experiment, an in situ X-Ray diffraction study versus temperature was performed under air and also under reductive atmosphere. Accordingly, the sample was heated from room temperature to 1073K and then cooled to room temperature under two different atmospheres.

Under Air: Figure 4a) shows diffractograms measured on the polycrystalline sample of $La_3Fe(MoO_4)_6$. All detected X-Ray lines are consistent with the orthorhombic unit cell of the studied phase. With increasing temperature one can notice: 1- a displacement of peaks positions related to a modification of the b-axis parameter occurring suddenly around 523K (figure 4c)) whereas no significant modification of a and c parameters are observed apart from ad

classical dilatation phenomenon and 2- above 523K some extra peaks appear (for instance at 23.36, 23.89 and 29.66°). This phenomenon is reversible on cooling and may be due to a partial decomposition of the tittle phase leading to a modification of *b*-parameter and with appearance of a new phase. A more detailed study is out of the scope of this preliminary study. After this accident, the refinement of unit cell parameters indicates a classical evolution with heating and cooling (Fig. 4). This temperature evolution of both the cell volume and of the different lattice constants, allowed the determination of the volume and of the linear thermal expansion coefficients α: α_V=28.6 10^{-6}, α_a=11 10^{-6}, α_b=16.1 10^{-6}, α_c=14.5 10^{-6} (K^{-1}). The thermal expansion of the material appears isotropic in all directions.

It is well known that iron molybdates may exhibit interesting magnetic properties depending on the connectivity and dimensionality between FeO_6 and MoO_4 subunits. For instance, (Cs,Rb)$Fe(MoO_4)_2$ is an example of triangular antiferromagnet with onset of 120° long range magnetic order below 4.5K. It was announced as a possible multiferroic type II material with

spontaneous polarization induced by the antisymmetric magnetic exchanges **[28][29]**. In $La_3Fe(MoO_4)_6$, the Fe connectivity is rather low and may suggest paramagnetism only. However, the present study shows a rather different signature, as detailed below.

The temperature dependence of the magnetic susceptibility of

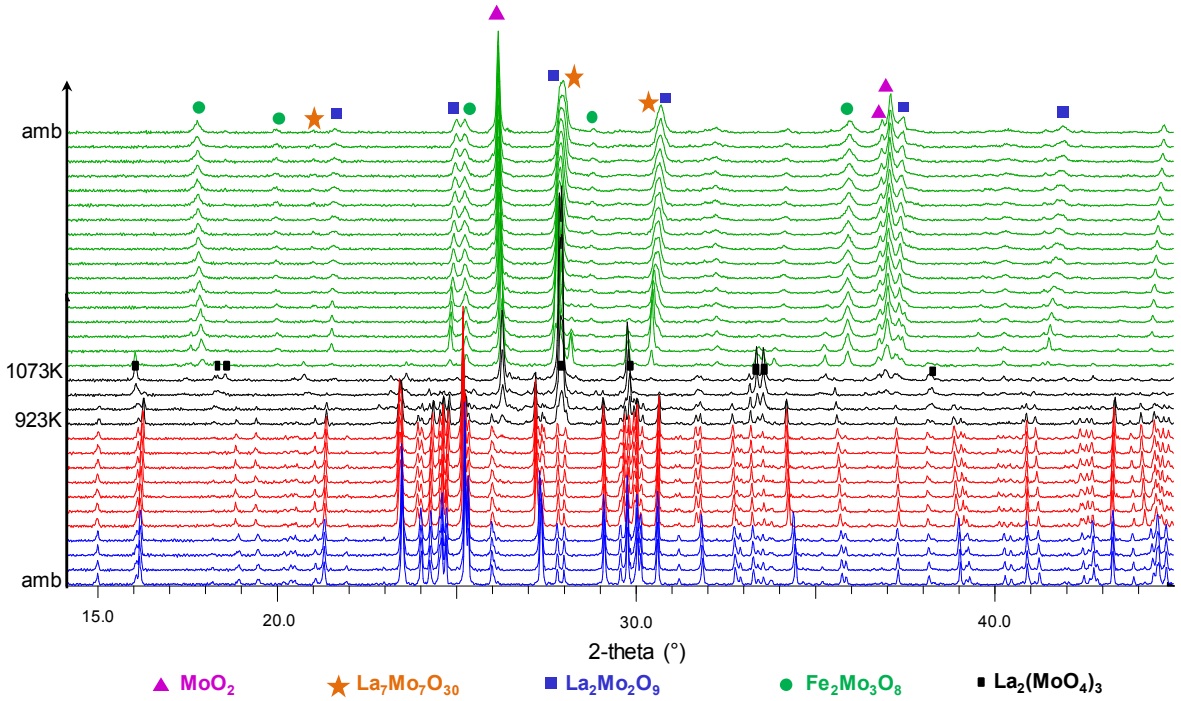

Figure 5: High-temperature X-ray diffraction data for $La_3Fe(MoO_4)_6$ measured under reductive atmosphere (N_2/3%H_2). The studied compound shows a phase transition at 523K (from blue to red part). Then, a transitional phase appears (in black) up to 1073K after which iron and molybdenum are reduced (green part).

This study is also the proof that the High Temperature form of $La_3Fe(MoO_4)_6$ has been stabilized and refined in this paper.

Under reductive atmosphere: The stability under a reductive environment was checked by in situ X-ray diffraction of the $La_3Fe(MoO_4)_6$ powder sampled heated under H_2/N_2 reductive atmosphere (figure 5). Under this atmosphere, the material is stable until 523K, temperature at which the same phenomenon as under air is observed. Above 923K, it starts to reduce to $La_2(MoO_4)_3$ and to an intermediate phase containing iron. Another reduction is observed during the cooling process, and leads to the formation of $La_7Mo(IV,V)_7O_{30}$, $MoIVO_2$, $La_2Mo_2O_9$ and $Fe(II)_2Mo(IV)_3O_8$.

Magnetic properties

polycrystalline $La_3Fe(MoO_4)_6$ is shown on figure 6. It evidenced a paramagnetic behaviour until a Neel like anomaly at T_N= 6.6 K. Below this anomaly, AFM ordering occurs despite the poor connectivity of the Fe sub lattice (Fe-Fe = 9.65Å along a, 5.25Å along b, 11.03Å along c). The curie-Weiss law was refined between 300K and 25 K law giving μ_{eff} = 6.2μB/Fe^{3+} and θ_{CW} = -13.8 K. The μ_{eff} value is slightly higher than the theoretical value (μ_{eff} = 5.92μB/Fe^{3+}), probably related with the presence of small impurities (the Morin transition of hematite is detected on χ^{-1} (T) at 260K). The low negative value of θ_{CW} is in good agreement with expected AFM ordering below TN. The magnetization at 2 K shown on insert of figure 6 is coherent with an AFM behaviour but shows an anomaly occurring at μ_0H ~ 2 Tesla, which could be due to minor Fe_2O_3 impurity. In this dilute Fe^{3+} system, the magnetic structure of $La_3Fe(MoO_4)_6$ is particularly interesting and especially the orientation and values of local moments of Fe^{3+} ions, in order to

conclude on the effects induced by very indirect exchanges Fe-$(O)_n$-Fe.

A neutron diffraction study was performed at low temperature (from RT to 1.5K) on the G41 diffractometer, LLB laboratory, Orsay, France. The onset of the magnetic ordering was confirmed through the appearance of magnetic satellites between 4K and 1.5K on the neutron diffractograms. The three main magnetic peaks appear at 14.86° (011), 16.44° (111) and 20.78° (211) and can be indexed in the crystal unit cell (propagation vector: k = (0,0,0)).

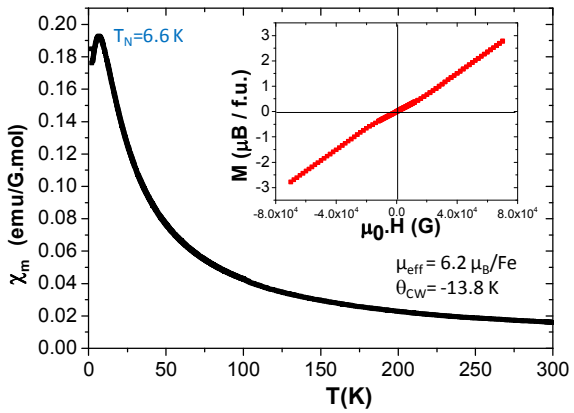

Figure 6: ZFC/FC plots of M/H versus temperature at 103 Gauss. It shows a paramagnetic behavior down to the Neel temperature: T_N= 6.6 K. Inset: magnetization M(H) at T=2 K in mB/f.u.(G).

There is one single magnetic ion (Fe^{3+}) in the Pbca unit cell, on Wyckoff site 8c (x, y, z). A symmetry analysis performed using the propagation vector k = 000, on the Pbca space group at site 8c shows that the magnetic components of all 8 sites are related by symmetry:

the magnetic representation Γ can be decomposed into 8 irreducible representations of dimension 1, contained 3 times each in Γ : $\Gamma = 3\Gamma_1 + 3\Gamma_2 + 3\Gamma_3 + 3\Gamma_4 + 3\Gamma_5 + 3\Gamma_6 + 3\Gamma_7 + 3\Gamma_8$.

To solve the magnetic structure, only the M_x M_y and M_z component of a single site, and the appropriate representation, are therefore needed. Only two representations lead to calculated magnetic intensities in relation with the experimental patterns Γ_3 and Γ_7.

$$\Gamma_3: \begin{matrix} S_1^x - S_2^x + S_3^x - S_4^x - S_5^x + S_6^x - S_7^x + S_8^x \\ S_1^y - S_2^y - S_3^y + S_4^y - S_5^y + S_6^y + S_7^y - S_8^y \\ S_1^z + S_2^z + S_3^z + S_4^z - S_5^z - S_6^z - S_7^z - S_8^z \end{matrix}$$

$$\Gamma_7: \begin{matrix} S_1^x + S_2^x + S_3^x + S_4^x - S_5^x - S_6^x - S_7^x - S_8^x \\ S_1^y + S_2^y - S_3^y - S_4^y - S_5^y - S_6^y + S_7^y + S_8^y \\ S_1^z - S_2^z + S_3^z - S_4^z - S_5^z + S_6^z - S_7^z + S_8^z \end{matrix}$$

where S_i^d is the component along the d-axis of atom Fe_i. These two representations differ by spin reversal of half of the Fe ions , i.e. S1, S4, S5 and S7. Taking into account the very weal magnetic satellites, the agreement factors are overestimated and should be carefully considered. However the best refinement was obtained with the representation Γ_7 (R_{magn} =24.9%) compared to Γ_3 (R_{magn} = 38.5%). In addition due to its very low value the S_y component was considered in a second stage, and its refinement in the Γ_3 model is unstable and does not converge. It follows that Γ_7 appears most plausible leading

Figure 7: a) NPD study at 4K and 1.5K. Main magnetic Bragg reflections are

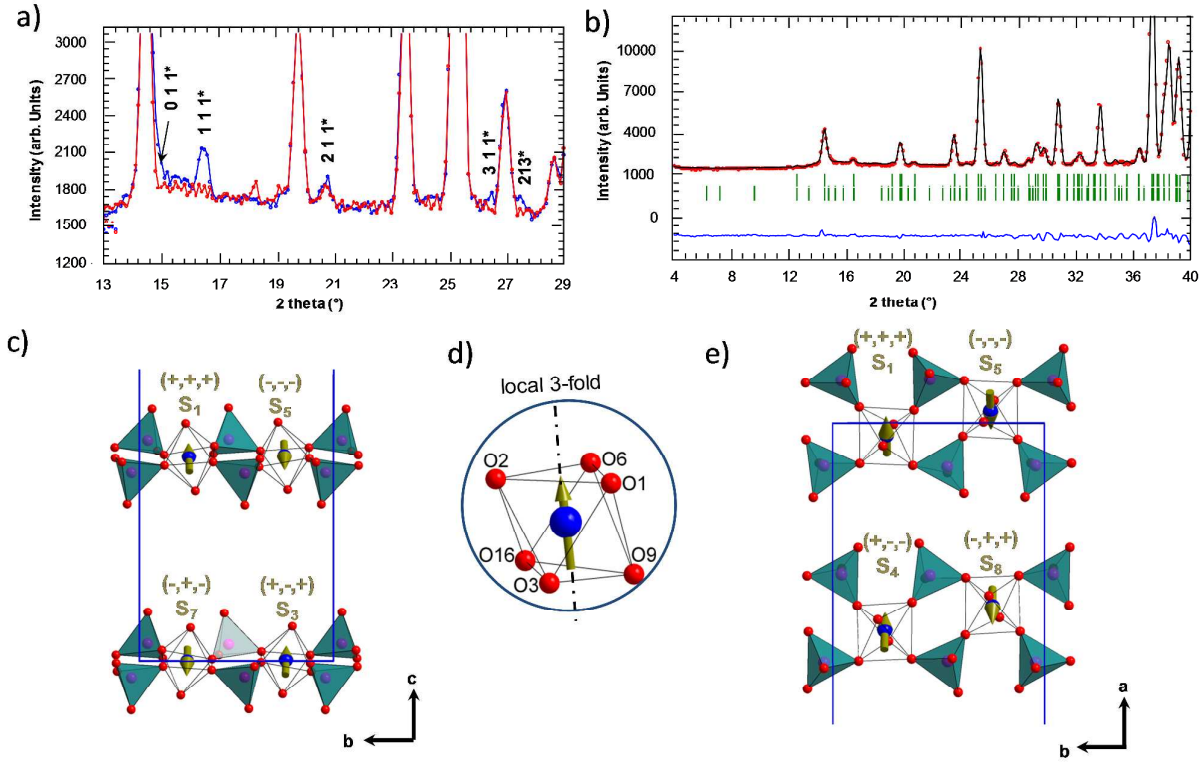

labelled, b) refinement of the neutron diffraction pattern at 1.5K using the obtained magnetic structure (k= (0,0,0)), orientation of magnetic moments in c) (a,b) and d) (a,c) planes. Local 3-flod geometry of magnetic moment in polyhedral is also enhanced.

to S^x =0.9(1), S^y=0.0(1), S^z =0.7(1) and M =1.2(1)μ_B. The calculated pattern is shown in figure 7. The refined magnetic structure is also shown in figure 7. Along the chains nearly parallel to the b-axis two consecutive FeO6 (Fe_1 and Fe_5) are antiferromagnetically coupled by Fe-O-O-Fe superexchanges (d(Fe-Fe) =5.25 Å). Between two chains separated by a/2 (e.g. Fe_1 and Fe_4), the spin components S_x are conserved while S_y and S_z are inversed. Finally, along c/2 (e.g. Fe_1 and Fe_7) only the weak S_y component is not reversed which corresponds to an almost total spin reversal. We note that along these two later directions magnetic coupling are very weak since no O_{2p} overlapping is expected taking into account long Fe-Fe distances (> 9Å) and Fe-O-O-O-O-Fe paths. One should here consider long-distance local dipole-dipole magnetic interactions at the origin of the 3D-ordering. The Γ_3 model considered above would be similar after shifting the spins of the chains by b/2. These weak exchanges are responsible for the very low T_N value and the weak magnetic moments refined at T=1.5 K show the setting of antiferromagnetic ordering with partially ordered moments. The particular orientation of the spins along the pseudo-3 fold axis of $Fe^{3+}O_6$ tetrahedra is surprising. For such isotropic magnetic ions (Fe^{3+}, d^5, L=0, no LS coupling), ions spin orientation is not expected to be influenced by local axes (i.e., orbital overlapping), but should rather be hold by crystal axes **[30]**,**[31]**. In $La_3Fe(MoO_4)_6$, most of the magnetic interactions are so weak, except along the chain AFM directions, that local symmetry could predominate. Indeed, it was shown very recently that the myth of isotropic Cu^{2+} ion (S=1/2) has to be revised for a more magneto-anisotropic model due to the spin-orbit coupling associated with their crystal-field split d-states**[32]**. Similar effects could be responsible for anisotropic Fe^{3+} local moments in the title compound.

Catalytic properties

Two samples of $La_3Fe(MoO_4)_6$ - described hereafter - were tested for the ethanol oxidation reaction at 600, 625 and 650K. For all the experiments, the carbon balance was always in the range of 100 $^{+}/_{-}$3 %. The first one was a $La_3Fe(MoO_4)_6$ sample used as-prepared (at high temperature and hence with big crystal sizes, figure 8a)), while the second one resulted from mechanically ball milling of the same solid prior to the catalytic test (in order to decrease the crystal size and hence to increase the specific area and thus reactivity, figure 8b)). After synthesis, the material was attrited 4 hours (Netzch PE 075, 1000 rpm) in ethanol using zirconia balls (2 mm diameter). This treatment leads to an increase in the SSA, of which the evolution over time is given in Table S4. Note that an efficient attrition procedure needs at least 20 g of powder.

Fig. 8 represents the evolution of the ethanol conversion versus the temperature for both samples (i.e., native and after 4 hours of attrition). As expected, the ethanol conversion increased with temperature. However, while, e.g., at 650K over the attrited $La_3Fe(MoO_4)_6$ powder a 97% ethanol conversion was observed, the native non-premilled $La_3Fe(MoO_4)_6$ sample was less active with a conversion of only 34% in the same conditions due to a lower SSA (0.4 m^2/g vs. 5.6 m^2/g for the former - Table S4). Ethanol oxidation on non-attrited $La_3Fe(MoO_4)_6$ exclusively leads to the production of a chemical product obtained after partial oxidation, namely acetaldehyde. Over the ball-milled sample other products were observed (Fig.8). The main product was still acetaldehyde, but CO_2 and formaldehyde were also formed. To explain the apparition of formaldehyde, we propose the following interpretation: the $CH_3CH(OH)CH_2COH$ aldol can be formed from ethanol and then retroaldolised to formaldehyde and acetone, as already reported **[33]**.

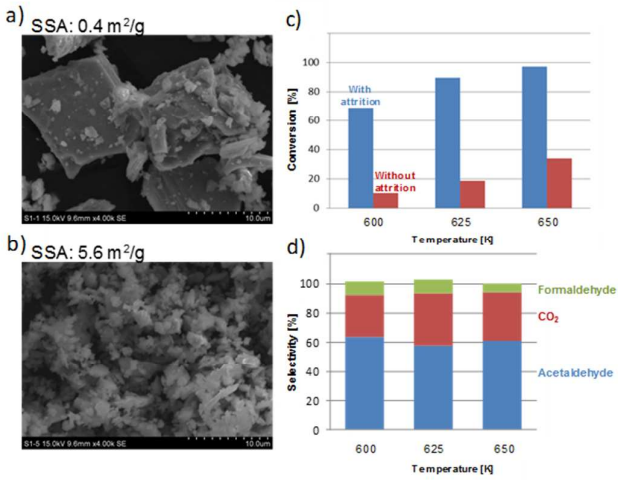

Figure 8: SEM micrographs of a $La_3Fe(MoO_4)_6$ sample prepared by solid state reaction a) before and b) after 4 hours attrition with precision of specific surface area (SSA), c) comparison of ethanol conversion for $La_3Fe(MoO_4)_6$ prepared with and without attrition and d) selectivity to different products for $La_3Fe(MoO_4)_6$ prepared with attrition.

For comparison, we also measured under the same conditions the performances of an industrial FeMo catalyst (with a comparable SSA of 6 $m^2.g^{-1}$) conventionally used for formaldehyde production from methanol **[34]–[37]**. Fig. 9 gives the products selectivity as a function of the reaction temperature for this sample. Full conversion (100%) of ethanol was observed for the whole range of temperatures. At 600K, the main product was acetaldehyde (i.e., selectivity of 55%). An increase in temperature led to the formation of other products such as carbon dioxide, formaldehyde, diethyl ether, furan, etc., which was detrimental for acetaldehyde selectivity. This was not observed on the $La_3Fe(MoO_4)_6$, which keeps a good selectivity to acetaldehyde when increasing temperature.

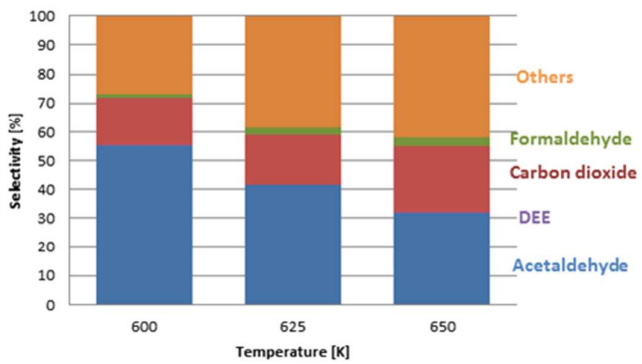

Figure 9: Comparison of selectivity to different products for FeMo catalyst in different temperatures

Conclusions

The second lanthanum iron molybdenum oxide referenced to date has been synthesized as a single crystal and pure powder.

Its composition (Fe+Mo for redox and La for basicity) and its stability in temperature under several atmospheres are in favour of potential catalytic applications. Preliminary results of ethanol reactivity conversion are very promising because the title compound exhibits, after only a simple mechanical attrition milling, a conversion rate of almost 100% with a good selectivity to acetaldehyde (and rather low amount of CO_2). In comparison with a conventional FeMo catalyst, the new $La_3Fe(MoO_4)_6$ is more selective for acetaldehyde production, even at high temperatures. Beside these catalytic properties, some antiferromagnetic properties have also been highlighted. We believe that the approach given in this manuscript is a good example of exploratory research enabling the prospection of new compounds with targeted properties, in different fields of applications.

Acknowledgements

The Fonds Europeeen de Developpement Regional (FEDER), CNRS, Region Nord Pas-de-Calais, and Ministere de l'Education Nationale de l'Enseignement Superieur et de la Recherche are acknowledged for funding the X-ray diffractometers. Laurence Burylo and Nora Djellal are thanked for their precious technical help. This work was carried out under the framework of the Multi-InMaDe project supported by the ANR (Grant ANR 2011-JS-08 003 01). Authors are grateful to Dr S. Colis for magnetic measurements..

Notes and references

.

[1] K. M. Ok, E. O. Chi, and P. S. Halasyamani, "Bulk characterization methods for non-centrosymmetric materials: second-harmonic generation, piezoelectricity, pyroelectricity, and ferroelectricity," *Chem. Soc. Rev.*, vol. 35, no. 8, pp. 710–717, Jul. 2006.

[2] P. S. Halasyamani, D. O'Hare, R. I. Walton, and D. W. Bruce, "Functional Oxides," John Wiley & Sons, Ltd, 2010, pp. pp. 1–39.

[3] S. D. Nguyen, J. Yeon, S.-H. Kim, and P. S. Halasyamani, "BiO(IO3): A New Polar Iodate that Exhibits an Aurivillius-Type (Bi2O2)2+ Layer and a Large SHG Response," *J. Am. Chem. Soc.*, vol. 133, no. 32, pp. 12422–12425, août 2011.

[4] A. Aliev, V. M. Kovrugin, M. Colmont, C. Terryn, M. Huvé, O. I. Siidra, S. V. Krivovichev, and O. Mentré, "Revised Bismuth Chloroselenite System: Evidence of a Noncentrosymmmetric Structure with a Giant Unit Cell," *Cryst. Growth Des.*, vol. 14, no. 6, pp. 3026–3034, juin 2014.

[5] D. Endara, M. Colmont, M. Huvé, F. Capet, J. Lejay, P. Aschehoug, and O. Mentré, "Inorganic polar blocks into controlled acentric assemblies," *Inorg. Chem.*, vol. 51, no. 17, pp. 9557–9562, Sep. 2012.

[6] F. Abraham, J. C. Boivin, G. Mairesse, and G. Nowogrocki, "The bimevox series: A new family of high performances oxide ion conductors," *Solid State Ion.*, vol. 40–41, Part 2, pp. 934–937, Aug. 1990.

[7] ebrary, Inc, *Biorefinery from biomass to chemicals and fuels*. Berlin ; Boston: Walter de Gruyter, 2012.

[8] I.-C. Marcu, D. Tichit, F. Fajula, and N. Tanchoux, "Catalytic valorization of bioethanol over Cu-Mg-Al mixed oxide catalysts," *Catal. Today*, vol. 147, no. 3–4, pp. 231–238, Oct. 2009.

[9] F. Hosoglu, J. Faye, K. Mareseanu, G. Tesquet, P. Miquel, M. Capron, O. Gardoll, J.-F. Lamonier, C. Lamonier, and F. Dumeignil, "High resolution NMR unraveling Cu substitution of Mg in hydrotalcites–ethanol reactivity," *Appl. Catal. Gen.*

[10] K. Thavornprasert, B. de la Goublaye de Ménorval, M. Capron, J. Gornay, L. Jalowiecki-Duhamel, X. Sécordel, S. Cristol, J.-L. Dubois, and F. Dumeignil, "Selective oxidation of ethanol towards a highly valuable product over industrial and model catalysts," *Biofuels*, vol. 3, no. 1, pp. 25–34, Jan. 2012.

[11] X. He and H. Liu, "Efficient synthesis of 1,1-diethoxyethane via sequential ethanol reactions on silica-supported copper and H-Y zeolite catalysts," *Catal. Today*, vol. 233, pp. 133–139, Sep. 2014.

[12] T. Tsuchida, J. Kubo, T. Yoshioka, S. Sakuma, T. Takeguchi, and W. Ueda, "Reaction of ethanol over hydroxyapatite affected by Ca/P ratio of catalyst," *J. Catal.*, vol. 259, no. 2, pp. 183–189, Oct. 2008.

[13] C. Carlini, M. Marchionna, M. Noviello, A. M. Raspolli Galletti, G. Sbrana, F. Basile, and A. Vaccari, "Guerbet condensation of methanol with n-propanol to isobutyl alcohol over heterogeneous bifunctional catalysts based on Mg–Al mixed oxides partially substituted by different metal components," *J. Mol. Catal. Chem.*, vol. 232, no. 1–2, pp. 13–20, mai 2005.

[14] E. Shahbazali, "Biorefinery: from biomass to chemicals and fuels," *Green Process. Synth.*, vol. 2, no. 1, pp. 87–88, Feb. 2013.

[15] K. Thavornprasert, M. Capron, L. Jalowiecki-Duhamel, O. Gardoll, M. Trentesaux, A.-S. Mamede, G. Fang, J. Faye, N. Touati, H. Vezin, J.-L. Dubois, J.-L. Couturier, and F. Dumeignil, "Highly productive iron molybdate mixed oxides and their relevant catalytic properties for direct synthesis of 1,1-dimethoxymethane from methanol," *Appl. Catal. B Environ.*, vol. 145, pp. 126–135, février 2014.

[16] N. Pernicore, F. Lazzerin, G. Liberti, and G. Lanzavecchia, *Journal of Catalysis*, p. 293, 1969.

[17] D. E. Bugaris and H.-C. zur Loye, "Materials Discovery by Flux Crystal Growth: Quaternary and Higher Order Oxides," *Angew. Chem. Int. Ed.*, vol. 51, no. 16, pp. 3780–3811, 2012.

[18] V. Petricek, M. Dusek, and L. Palatinus, *Jana2006. The crystallographic computing system*. Praha, Czech Republic: Institute of Physics, 2006.

[19] *SAINT: Area-Detector Integration Software*. Madison: Siemens Industrial Automation, Inc., 1996.

[20] *SADABS: Area-Detector Absorption Correction.* Madison: Siemens Industrial Automation, Inc., 1995.

[21] L. Palatinus and G. Chapuis, "SUPERFLIP – a computer program for the solution of crystal structures by charge flipping in arbitrary dimensions," *J. Appl. Crystallogr.*, vol. 40, no. 4, pp. 786–790, Jul. 2007.

[22] G. V. Bazuev, V. G. Zubkov, and G. P. Shveikin, "New perovskite-relaxed mixed oxides Ln Fe2/3 Mo1/3 O3 (Ln= La, Ce, Pr, Nd):

Synthesis, structure, and properties," *Zhurnal Neorganicheskoi Khimii*, pp. 2000–2005, 1996.
[23] K. M. Khal'baeva, S. F. Solodovnikov, E. G. Khaikina, Y. M. Kadyrova, Z. A. Solodovnikova, and O. M. Basovich, "Phase formation features in the systems M2MoO4–Fe2(MoO4)3 (M=Rb, Cs) and crystal structures of new double polymolybdates M3FeMo4O15," *J. Solid State Chem.*, vol. 183, no. 3, pp. 712–719, Mar. 2010.
[24] M. Maczka, A. Pietraszko, G. D. Saraiva, A. G. S. Filho, W. Paraguassu, V. Lemos, C. A. Perottoni, M. R. Gallas, P. T. C. Freire, P. E. Tomaszewski, F. E. A. Melo, J. M. Filho, and J. Hanuza, "High pressure effects on the structural and vibrational properties of antiferromagnetic KFe(MoO4)2," *J. Phys. Condens. Matter*, vol. 17, no. 39, p. 6285, Oct. 2005.
[25] M. H. Rapposch, J. B. Anderson, and E. Kostiner, "Crystal structure of ferric molybdate, Fe2(MoO4)3," *Inorg. Chem.*, vol. 19, no. 11, pp. 3531–3539, Nov. 1980.
[26] T. Namsaraeva, B. Bazarov, D. Mikhailova, N. Kuratieva, A. Sarapulova, A. Senyshyn, and H. Ehrenberg, "Orthomolybdates in the Cs–FeII,III–Mo–O System: Cs4Fe(MoO4)3, Cs2Fe2(MoO4)3 and CsFe5(MoO4)7," *Eur. J. Inorg. Chem.*, vol. 2011, no. 18, pp. 2832–2841, juin 2011.
[27] S. V. Krivovichev, "Which Inorganic Structures are the Most Complex?," *Angew. Chem. Int. Ed.*, vol. 53, no. 3, pp. 654–661, Jan. 2014.
[28] T. Inami, "Neutron powder diffraction experiments on the layered triangular-lattice antiferromagnets RbFe(MoO4)2 and CsFe(SO4)2," *J. Solid State Chem.*, vol. 180, no. 7, pp. 2075–2079, 2007.
[29] A. Gągor, P. Zajdel, and D. Többens, "The phase transitions in CsFe(MoO4)2 triangular lattice antiferromagnet, neutron diffraction and high pressure studies," *J. Alloys Compd.*, vol. 607, pp. 104–109, Sep. 2014.
[30] R. David, H. Kabbour, S. Colis, and O. Mentré, "Slow Spin Dynamics between Ferromagnetic Chains in a Pure-Inorganic Framework," *Inorg. Chem.*, vol. 52, no. 23, pp. 13742–13750, 2013.
[31] B. C. Melot, G. Rousse, J.-N. Chotard, M. Ati, J. Rodríguez-Carvajal, M. C. Kemei, and J.-M. Tarascon, "Magnetic Structure and Properties of the Li-Ion Battery Materials FeSO4F and LiFeSO4F," *Chem. Mater.*, vol. 23, no. 11, pp. 2922–2930, 2011.
[32] J. Liu, H.-J. Koo, H. Xiang, R. K. Kremer, and M.-H. Whangbo, "Most spin-1/2 transition-metal ions do have single ion anisotropy," *ArXiv14092795 Cond-Mat*, Sep. 2014.
[33] J. Bussi, S. Parodi, B. Irigaray, and R. Kieffer, "Catalytic transformation of ethanol into acetone using copper–pyrochlore catalysts," *Appl. Catal. Gen.*, vol. 172, no. 1, pp. 117–129, août 1998.
[34] E. Tronconi, A. S. Elmi, N. Ferlazzo, P. Forzatti, G. Busca, and P. Tittarelli, "Methyl formate from methanol oxidation over coprecipitated V-Ti-O catalysts," *Ind. Eng. Chem. Res.*, vol. 26, no. 7, pp. 1269–1275, juillet 1987.
[35] G. Deo and I. E. Wachs, "Reactivity of Supported Vanadium Oxide Catalysts: The Partial Oxidation of Methanol," *J. Catal.*, vol. 146, no. 2, pp. 323–334, avril 1994.
[36] I. E. Wachs, *US Patent*, p. 6875724, 2005.
[37] J. Gornay, X. Secordel, M. Capron, G. Tesquet, P. Fongarland, E. Payen, J. L. Dubois, and F. Dumeignil, "Synthèse directe du 1,1-diméthoxyméthane à partir de méthanol moyennant une modification mineure du procédé de production de formaldéhyde sur catalyseurs FeMo," *Oil Gas Sci. Technol. – Rev. D'IFP Energ. Nouv.*, vol. 65, no. 5, pp. 751–762, Sep. 2010.

Table Of Content

Novel $La_3Fe(MoO_4)_6$ oxide phase: magnetic properties and ethanol reactivity

Marie Colmont, Georgiana Bucataru, Marielle Huvé, Anita Borowiek , Mickaël Capron, Franck Dumeignil, Frédéric Capet, Françoise Damay, Olivier Mentré and Pascal Roussel

This paper reports the synthesis, crystal structure and properties of the new $La_3Fe(MoO_4)_6$ phase. A neutron study enabled refinement of the magnetic structure evidencing AFM coupling at 1.5K. It also exhibited a promising ethanol conversion with a better selectivity to acetaldehyde than a conventional FeMo.